

## MIT Open Access Articles

*Nanopatterned Electrically Conductive  
Films of Semiconductor Nanocrystals*

The MIT Faculty has made this article openly available. **Please share** how this access benefits you. Your story matters.

**Citation:** Mentzel, Tamar S., Darcy D. Wanger, Nirat Ray, Brian J. Walker, David Strasfeld, Mounji G. Bawendi, and Marc A. Kastner. "Nanopatterned Electrically Conductive Films of Semiconductor Nanocrystals." *Nano Letters* 12, no. 8 (August 8, 2012): 4404-4408.

**As Published:** <http://dx.doi.org/10.1021/nl3022863>

**Publisher:** American Chemical Society

**Persistent URL:** <http://hdl.handle.net/1721.1/79791>

**Version:** Author's final manuscript: final author's manuscript post peer review, without publisher's formatting or copy editing

**Terms of Use:** Article is made available in accordance with the publisher's policy and may be subject to US copyright law. Please refer to the publisher's site for terms of use.



# Nanopatterned, Electrically Conductive Films of Semiconductor Nanocrystals

Tamar S. Mentzel,<sup>\*,†</sup> Darcy D. Wanger,<sup>‡</sup> Nirat Ray,<sup>†</sup> Brian Walker,<sup>‡</sup> David  
Strasfeld,<sup>‡</sup> Mounji G. Bawendi,<sup>‡</sup> and Marc A. Kastner<sup>†</sup>

*Department of Physics, Massachusetts Institute of Technology, Cambridge, Massachusetts 02139,  
and Department of Chemistry, Massachusetts Institute of Technology, Cambridge, Massachusetts  
02139*

E-mail: tamarm@mit.edu

**KEYWORDS:** Semiconductor nanocrystals, nanopatterning, electron beam lithography, quantum dots, charge transport

## Abstract

We present the first semiconductor nanocrystal films of nanoscale dimensions that are electrically conductive and crack-free. These films make it possible to study the electrical properties intrinsic to the nanocrystals unimpeded by defects such as cracking and clustering that typically exist in larger-scale films. We find that the electrical conductivity of the nanoscale films is 180 times higher than that of drop-casted, microscopic films made of the same type of nanocrystal. Our technique for forming the nanoscale films is based on electron-beam lithography and a lift-off process. The patterns have dimensions as small as 30 nanometers, and are positioned on a surface with 30-nanometer precision. The method is flexible in the choice of nanocrystal core-shell materials and ligands. We demonstrate patterns with PbS, PbSe, and

---

\*To whom correspondence should be addressed

<sup>†</sup>Department of Physics, Massachusetts Institute of Technology, Cambridge, Massachusetts 02139

<sup>‡</sup>Department of Chemistry, Massachusetts Institute of Technology, Cambridge, Massachusetts 02139

CdSe cores and  $Zn_{0.5}Cd_{0.5}Se$ - $Zn_{0.5}Cd_{0.5}S$  core-shell nanocrystals with a variety of ligands. We achieve unprecedented versatility in integrating semiconductor nanocrystal films into device structures both for studying the intrinsic electrical properties of the nanocrystals and for nanoscale optoelectronic applications.

The tunable electronic and optical properties of semiconductor nanocrystals and their low-cost solution processing make them attractive building blocks for designer solids and for various optoelectronic applications. However, it is only with nanoscale control of their assembly and placement on a surface that nanocrystal solids can be used for nanoelectronic and nanophotonic circuits,<sup>1</sup> LED nanodisplays,<sup>2,3</sup> diffraction gratings,<sup>4</sup> and the capture and detection of individual biomolecules.<sup>5,6</sup> Moreover, crack- and cluster-free nanocrystal films that are integrated into devices with nanoscale precision open the possibility of studying the nanoscopic electronic dynamics of these artificial solids. Investigating charge transport in the localized states of the nanocrystals is important for their application in optoelectronic devices, and more generally for acquiring a deeper understanding of charge transport in localized electronic states, which arise in technologically important materials such as amorphous semiconductors, organic materials and semiconductor nanostructures. Finally, eliminating structural defects in the films, such as cracks and clustering, and their effect on charge transport is an essential step toward realizing a nanocrystal solid that exhibits the predicted charge correlations.<sup>7</sup>

Prior methods for assembling nanocrystals into patterned structures on a substrate fall into three main categories. The first entails functionalizing the nanocrystals with a ligand to control the interaction between the nanocrystals and a surface. For example, nanocrystals can be photopatterned by functionalizing them with a photosensitive ligand that renders them insoluble when exposed to ultra-violet light.<sup>8-10</sup> Another example is by Tsuruoka *et al.* who immobilized nanocrystals on a surface by functionalizing the nanocrystal with a ligand that binds to the substrate.<sup>11</sup> These techniques do not form close-packed films, and the patterns are limited to microscale resolution. A second method uses a nanopatterned template that guides the assembly of the nanocrystals. Son *et al.* nanopatterned a block copolymer thin film, and assembled nanocrystals in the grooves on

the surface of the polymer film.<sup>12</sup> Another related technique takes advantage of capillary forces to drive nanocrystals into trenches etched into a substrate<sup>13</sup> or in a polymer film.<sup>14</sup> These techniques attain nanoscale control over the formation and placement of the nanocrystals on a specialized surface, but do not allow the integrated device fabrication necessary for the aforementioned applications. A third class of patterning techniques is printing: microcontact printing,<sup>2,4,15</sup> ink-jet printing,<sup>16</sup> and nano-imprint lithography of a nanocrystal-polymer composite.<sup>17</sup> Microcontact printing achieves nanoscale patterns, but it is highly sensitive to the chemical compatibility of the nanocrystal solution, the stamp and the substrate; the nanocrystals must preferentially adhere to the substrate over the polymer stamp, which tends to exclude prevalent device surfaces like silicon dioxide ostensibly because its hydrophilicity is incompatible with hydrophobic ligands. Moreover, stamps offer only limited control over the placement of the pattern onto the surface. Ink-jet printing eliminates the constraints on chemical compatibility that exist with a stamp, but at the cost of pattern resolution because droplets are 50-100  $\mu\text{m}$  in size. The challenge remains to form nanoscale films of semiconductor nanocrystals that can be integrated into a device structure with nanoscale precision.

An additional requirement of nanocrystal films for many of the aforementioned applications is that they be electrically conductive and free of structural defects such as cracks and clusters. When nanocrystals are drop-casted onto a surface, they tend to form clusters as shown in Figure 1(b). Experiments by Mics *et al.* indicate that when clustering is present, the measured conductivity of nanocrystal films differs from the intrinsic conductivity of the nanocrystals. As such, clustering diminishes the efficiency of charge transport in nanocrystal films in optoelectronic and other device applications. It also makes it impossible to study the charge dynamics intrinsic to the nanocrystals, and is thus a barrier to realizing nanocrystal-based designer solids.

In addition to clustering, cracks in the films can be a compounding problem. The electrical current in drop-casted nanocrystal films is typically immeasurably small because the electronic coupling between nanocrystals, as determined by the size of the native capping ligand, is weak.<sup>18-21</sup> To increase the coupling strength of the nanocrystals, either the film is annealed<sup>18,22,23</sup> or the na-

tive capping ligand on the nanocrystal is exchanged for a smaller molecule by immersing the film in a solution containing the smaller molecule.<sup>20,24,25</sup> In both of these approaches, there is a strong driving force that creates cracks in the film, adding to the structural defects. [ Figure 1(c) shows an annealed film]. Despite the clusters and cracks, it has been possible to study charge transport in these films because current may flow through a continuous pathway that connects the clusters; or, a second layer of nanocrystals can be deposited to fill in the voids between clusters.<sup>20</sup> All studies of charge transport that we are aware of have been performed on films of micrometer dimensions or larger, and involve annealing or a ligand exchange, which makes it likely that structural defects are influencing the transport properties. Eliminating structural defects is important for investigating the intrinsic charge transport properties and for optimizing the transport efficiency in micron-scale films or larger, and in nanoscale films it is essential for enabling charge transport of any kind. When voids of the order of tens or hundreds of nanometers arise in nanopatterned films, a complete break in the film can make it impossible for charge to flow at all.

In this Letter, we present semiconductor nanocrystal films of nanoscale dimensions that are electrically conductive without clustering or cracks. To assemble the nanocrystals into nanoscale patterns, we use electron-beam lithography followed by nanocrystal deposition and lift-off. The technique uniquely combines the following characteristics: nanocrystal films with features as small as 30 nm; controlled placement of nanocrystal films onto a surface or into a device structure with nanoscale precision ( $\approx 30$  nm); flexibility in choice of nanocrystal core material, ligand, and solvent; flexibility in the choice of substrate; and structurally continuous films with a measurable electrical current. We perform electrical measurements of these films and find that the electrical conductivity is 180 times higher than what is found in larger-scale films. The nanoscale size of the film is essential to eliminating defects so that we can measure the intrinsic electronic properties of the nanocrystals. With these nanopatterned films, it is now possible to probe the electronic dynamics of an ordered array of localized sites formed by the nanocrystals and to incorporate nanocrystal films into nanoelectronic and nanophotonic circuits as well as nanoscale optoelectronic devices and sensors.

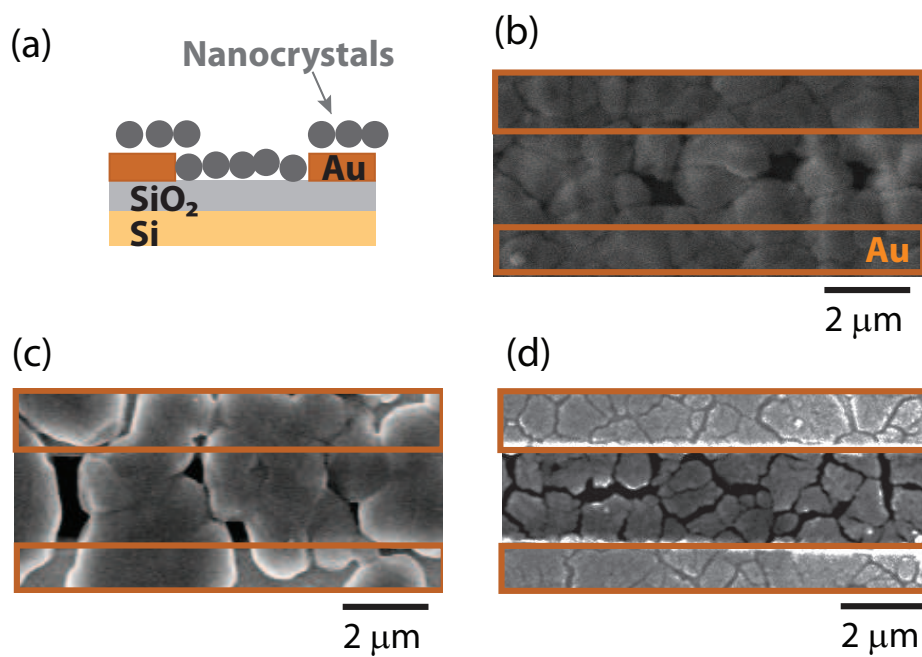


Figure 1: (a) Schematic of nanocrystals drop cast on an inverted FET device (side view). (b) Scanning electron micrograph of a PbSe nanocrystal film drop cast on an inverted FET device (top view; the gold electrodes, which appear beneath the nanocrystal film, are outlined in orange), and (c) after annealing the film for one hour at 400 K. (d) When the thickness of the film exceeds approximately 1 micron, cracks emerge as the film dries, namely as solvent interior to the film evaporates and diffuses to the already dry surface.

The following describes the process for forming electrically conductive, crack-free nanocrystal films of nanoscale dimensions. Here we discuss the preparation of PbS nanocrystal films,[ Figure 2] and the same approach holds for films of other types of nanocrystal. We choose silicon dioxide as a substrate on which to pattern the films because of its prevalence in a variety of device applications. On a substrate approximately 5 mm  $\times$  5 mm, we spin coat a 100-nm-thick layer of positive resist for electron-beam lithography. We pattern nanoscale trenches in the PMMA of arbitrary shape and size as small as 30 nm.

The next step is to drop cast nanocrystals into the nanopatterned trenches. PbS nanocrystals are prepared by high-temperature pyrolysis of Pb and S precursors in an oleic acid/octadecene mixture.<sup>26,27</sup> Before drop-casting, we process the growth solution to remove remaining salts and byproducts and to exchange the native capping ligand for a smaller molecule. Exchanging the capping ligand while the nanocrystals are still in solution is critical for making films with a measurable current and free of the cracks caused by annealing or by exchanging the ligand once the film is formed. Processing occurs in the nitrogen environment of a glovebox according to a modified version of a previously reported method.<sup>24</sup> A mixture of methanol and butanol is added to the solution to precipitate the nanocrystals. The sample is centrifuged to collect the nanocrystals and the supernatant is discarded. The nanocrystals are redissolved in hexane and are precipitated a second time in a mixture of methanol and butanol and redissolved in a solution of *n*-butylamine (C<sub>4</sub>H<sub>11</sub>N). After stirring the solution for approximately 72 hours, the native cap of oleic acid ( $\approx$ 1.8 nm long) is completely replaced with *n*-butylamine ( $\approx$ 0.6 nm long).<sup>28,29</sup> The nanocrystals are precipitated a third time with isopropanol, redissolved in a 9:1 hexane:octane mixture, and passed through a 0.1  $\mu$ m filter. In Figure 2, transmission electron micrographs (TEM) of a monolayer of PbS nanocrystals before and after exchanging the ligand reveal decreased inter-nanocrystal spacing with the *n*-butylamine cap, as expected.

Drop-casting the nanocrystals into the trenches and lift-off are performed in the glovebox. We tune the concentration of nanocrystals in solution to  $\approx$ 85  $\mu$ mol per liter. We drop cast 1  $\mu$ L of this solution on the surface and allow it to dry for ten minutes. For lift-off, we put the substrate into a

vial of acetone to dissolve the remaining PMMA, leaving a 50-nm-thick film of nanocrystals on the substrate whose shape is defined by the pattern in the PMMA. In traditional lift-off processes, care is taken to avoid depositing the film on the sidewalls of the PMMA. In contrast, the hydrophobic ligands on the surface of the nanocrystals have an affinity for the PMMA and coat the sidewalls of the trenches patterned in the PMMA. To ensure that the nanocrystal film tears cleanly at the boundary of the patterns, we sonicate the substrate in the vial of acetone for three seconds. Longer sonication times may cause tears in nanoscale features of the film.

The resulting films are robust and remain bound to the surface even when immersed in non-polar solvents like hexane or octane in which the nanocrystals are normally soluble. We hypothesize that during the lift-off process, acetone removes the ligands from the surface of the nanocrystals on the outermost layer of the film rendering the film insoluble. We speculate that the ligand is being removed from only the top layer because the nanopatterned films fluoresce (as shown in Figures 3 and 4), which would not be the case if the ligands were absent. More details on the patterning process can be found in the Supporting Information.

In Figures 3 and 4, we demonstrate films made from PbS nanocrystals with *n*-butylamine ligands, PbSe nanocrystals with oleic acid ligands, CdSe nanocrystals with phosphonic acid ligands, and Zn<sub>0.5</sub>Cd<sub>0.5</sub>Se-Zn<sub>0.5</sub>Cd<sub>0.5</sub>S core-shell and phosphonic acid ligands. In Figure 4(b) the nanoscale pattern of nanocrystals is placed with nanoscale precision relative to a nearby transistor gate. Our patterns are as small as 30 nm in size. [ Figure 4(c)]. By adjusting the concentration of nanocrystals in solution, we are able to tune the thickness of the nanocrystal pattern from 20 to 150-nm thick.

To measure the electrical conductance of the films, we pattern a nanocrystal film approximately 130 nm thick ( $\approx 22$  monolayers) between two gold electrodes, as shown in Figure 5(a). The pattern is 350 nm wide at its narrowest point, and from the current-voltage characteristic, which is Ohmic at low voltages [ Figure 5(b)], we find the zero-bias conductivity to be 17  $\mu\text{S}/\text{cm}$ . We pattern a second film that is rectangular with dimensions 50 nm thick, 2  $\mu\text{m}$  wide, and 1  $\mu\text{m}$  long and find that the conductivity is equal.



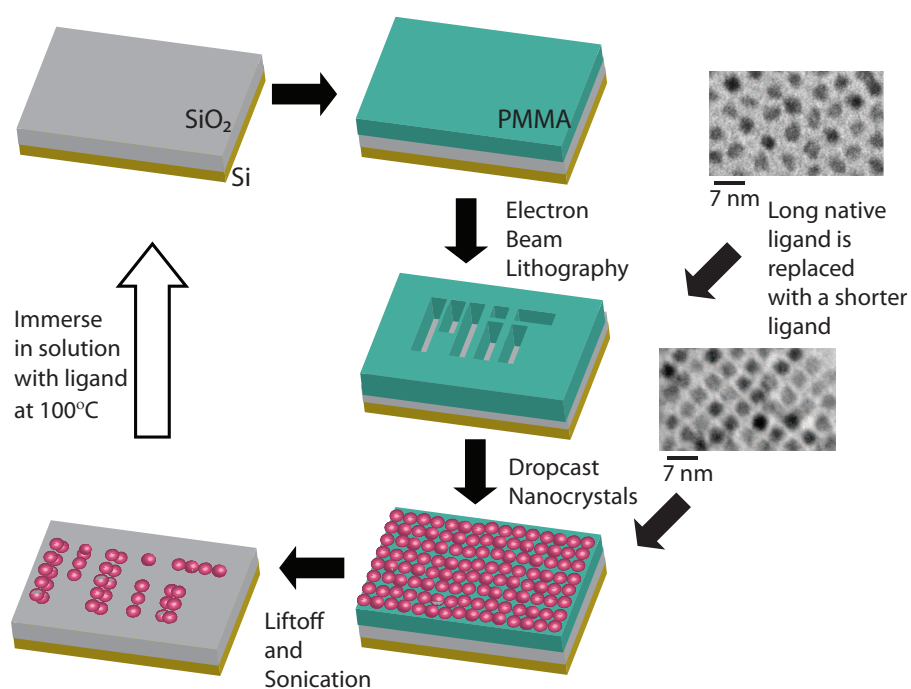


Figure 2: (Left and Center) An overview of the process for patterning nanoscale films of semiconductor nanocrystals. The patterns are positioned on the surface of the substrate with nanoscale precision. To achieve electrically conducting films without cracking the film by annealing or exchanging the capping ligand for a smaller molecule, we exchange the capping ligand while the nanocrystals are still in solution prior to deposition. (Right) Transmission electron micrographs of the nanocrystal films before and after cap exchange.

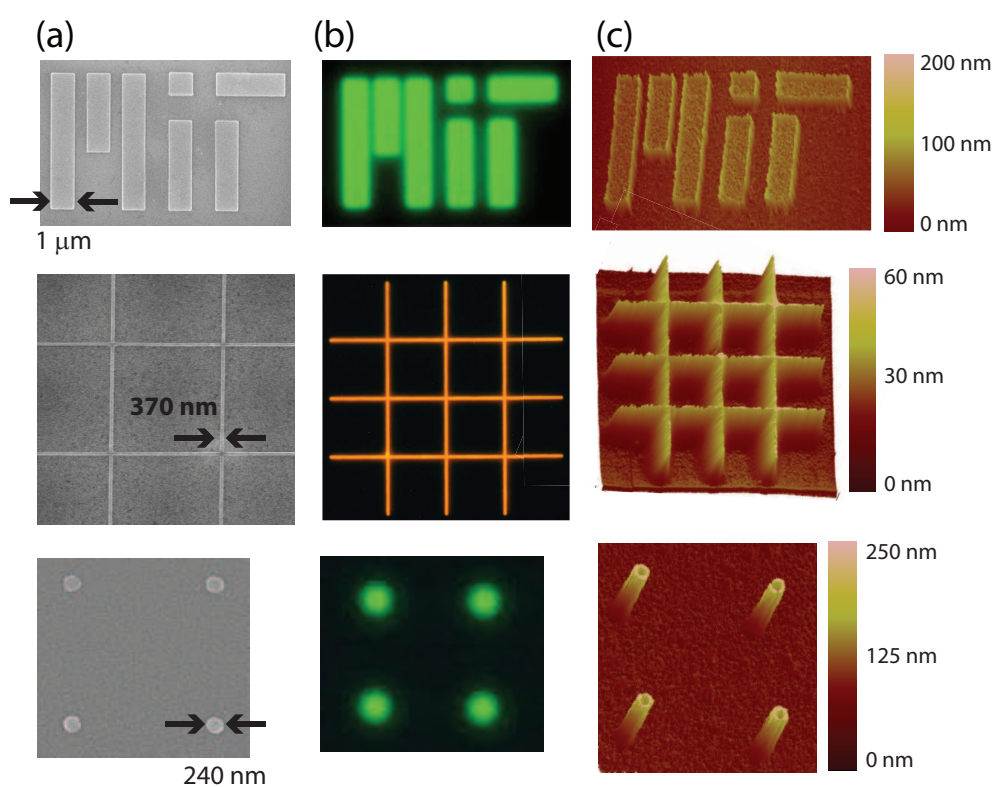


Figure 3: Nanopatterned films of CdSe (orange fluorescence) and  $\text{Zn}_{0.5}\text{Cd}_{0.5}\text{Se-Zn}_{0.5}\text{Cd}_{0.5}\text{S}$  core-shell (green fluorescence) nanocrystals. (a) Scanning electron micrograph, (b) fluorescence (actual color) and (c) AFM images.

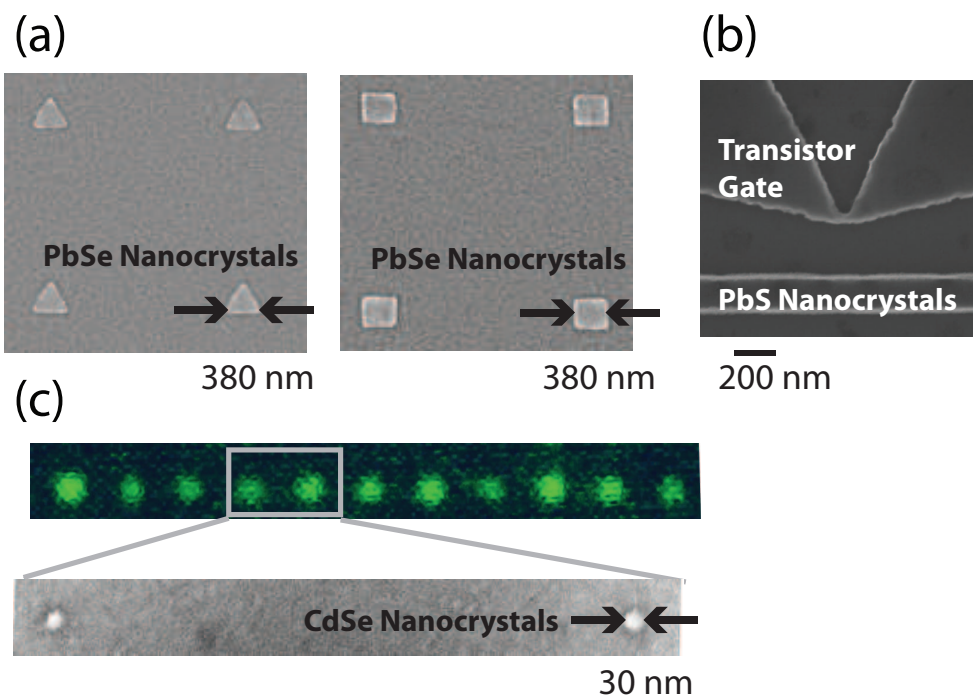


Figure 4: We demonstrate the flexibility in choice of nanocrystal materials by patterning films from (a) PbSe nanocrystals capped with oleic acid, (b) PbS nanocrystals capped with *n*-butylamine, and (c)  $Zn_{0.5}Cd_{0.5}Se-Zn_{0.5}Cd_{0.5}S$  core-shell nanocrystals capped with phosphonic acids. In (b), the PbS nanocrystal film is patterned to a nearby transistor gate with nanoscale precision. All of these images are scanning electron micrographs except in (c) where we show both green fluorescence and an electron micrograph indicating that the size of the pattern is only about 30 nm.

To compare the conductivity of the patterned films with drop-casted, microscopic films, we fabricate device structures of the kind illustrated in Figure 1(a) and drop cast on them the same PbS nanocrystals with an *n*-butylamine capping ligand. The morphology of the resulting films is as shown in Figure 1(b). We measure one film that is 300 nm thick, 800  $\mu\text{m}$  wide and 2  $\mu\text{m}$  long and two that are 40 nm thick, 800  $\mu\text{m}$  wide and 2 or 5  $\mu\text{m}$  long. We plot the conductance versus the dimensions of the films in Figure 5(c). The conductivity  $\sigma$  is calculated from the relationship  $G = \sigma \frac{lw}{l}$  where  $G$  is the conductance,  $l$  is the length,  $t$  is the thickness, and  $w$  is the width of the film. The plot illustrates that the conductivity of the crack-free, nano-patterned films is higher than the conductivity of the unpatterned, drop-casted films, which exhibit structural disorder.<sup>30</sup> The conductivity of the unpatterned, microscopic films is approximately 0.09  $\mu\text{S}/\text{cm}$ , a factor of 180 lower than the nanoscopic films. By eliminating the clustering, we uncover a new regime of charge transport in semiconductor nanocrystal films. Forthcoming work by the authors will explore this in greater detail.

Another technological benefit of our method for forming nanoscale films is that we are able to remove the patterned films from the substrate and to recycle the substrate if necessary. By submerging the substrate with the film in a solution of 19:1 octane:*n*-butylamine and heating it to 100°C overnight, the films dissolve into the solution. We chose octane as a solvent because its boiling point (125°C) is higher than that of other commonly used solvents like hexane (boiling point of 68°C), and the solution does not evaporate when we raise the temperature for a prolonged period. We believe that when we immerse the film in a heated solution containing the *n*-butylamine ligand, we drive the ligand back on the surface of the outermost layer of nanocrystals, first enabling the outermost layer of nanocrystals to redissolve in the solution and subsequently the remaining nanocrystals to do so as well.

We have demonstrated nanoscale patterns of semiconductor nanocrystals that are electrically conductive and structurally continuous. Using electron-beam lithography and lift-off, we achieve patterns with 30 nm resolution that can be integrated into a device structure with 30-nm precision. The process allows flexibility in the choice of nanocrystal core material, ligand and solvent

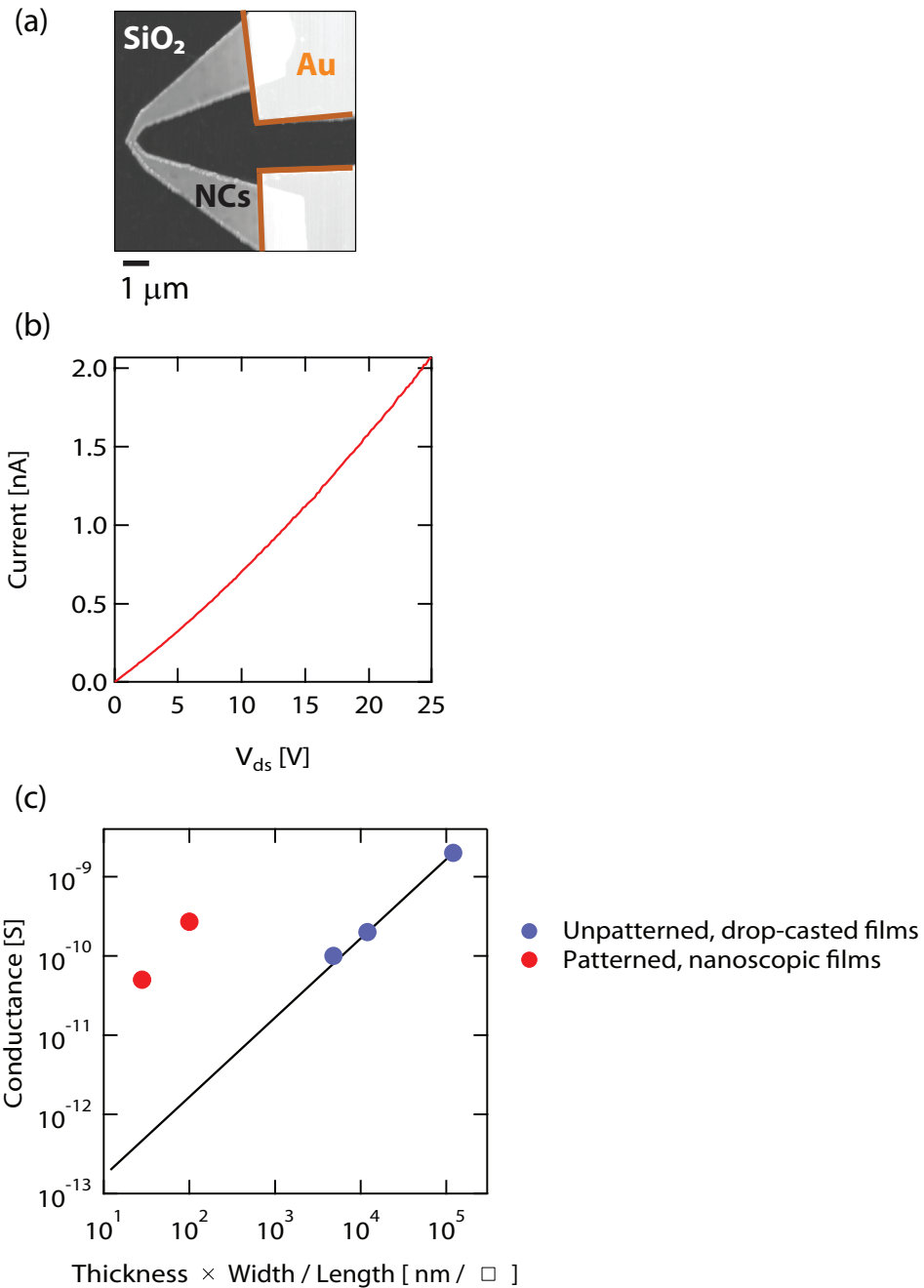


Figure 5: (a) An AFM image of a film of PbS nanocrystals capped with *n*-butylamine, which is 350 nm wide at its narrowest point. The film is continuous, in contrast to those shown in Figure 1. (b) IV characteristic of the nanopatterned film shown in (a). (c) Conductance of *n*-butylamine-capped PbS nanocrystals versus the dimensions of the film with  $V_{ds} = 0.1$  V. The red circles represent the conductance of the nanopatterned film shown in (a) and a comparable rectangular film with nanometer dimensions. The blue circles represent the conductance of a microscopic film in a device structure shown in Figure 1, and the dimensions of the film are 800 μm wide, between 40 and 300 nm thick, and either 2 or 5 μm wide. The conductivity of the nanoscopic films is 180 times higher than what is found in the microscopic films.

without constraints on the choice or design of the substrate. We have performed the first electrical measurements of nanocrystal films of nanoscale dimensions that are free of the clustering and cracks typically found in films of micrometer dimensions or larger. The electrical conductivity of the patterned, nanoscale films is 180 times higher than the conductivity of larger, drop-casted films in which the nanocrystals form clusters. This technique for patterning nanocrystal films opens the possibility of studying the nanoscopic charge dynamics in the localized states of the nanocrystals. Eliminating structural defects is an essential step toward realizing the charge correlations predicted in ordered nanocrystal arrays. Finally, the ability to control the formation of nanocrystal films with nanoscale resolution makes it possible to use nanocrystal films in applications such as nanoelectronics, nanophotonics, LED nanodisplays, and nanoscale detection of biomolecules.

## **Acknowledgement**

We are grateful to Mark Mondol and the RLE SEBL facility for experimental help with electron-beam lithography. This work was supported by the U.S. Army Research Office under contract W911 NF-07-D-0004 (patterning and electrical measurements of PbS nanocrystals) and by the Department of Energy under award number DE-FG02-08ER46515 (patterning and imaging of PbSe, CdSe and CdSe/ZnS nanocrystals) and by Samsung SAIT. D.D.W. gratefully acknowledges support from the Fannie and John Hertz Foundation Fellowship.

## **Supporting Information Available**

Details on the method for forming nanoscale patterns of semiconductor nanocrystals on a substrate. This material is available free of charge via the Internet at <http://pubs.acs.org/>.

## **References**

- (1) Olsson, Y.; Chen, G.; Rapaport, R.; Fuchs, D.; Sundar, V.; Steckel, J.; Bawendi, M. G.; Aharoni, A.; Banin, U. *Appl. Phys. Lett.* **2004**, *85*, 4469.

- (2) Kim, L.; Anikeeva, P. O.; Coe-Sullivan, S. A.; Steckel, J. S.; Bawendi, M. G.; Bulovic, V. *NanoLetters* **2008**, *8*, 4513–4517.
- (3) Bae, W. K.; Kwak, J.; Lim, J.; Lee, D.; Nam, M. K.; Char, K.; Lee, C.; Lee, S. *Nano Lett* **2010**, *10*, 2368–2373.
- (4) Shallcross, R. C.; Chawla, G. S.; Marikkar, F. S.; Tolpert, S.; Pyun, J.; Armstrong, N. *ACS Nano* **2009**, *3*, 3629–3637.
- (5) Pattani, V. P.; Li, C.; Desai, T. A.; Vu, T. Q. *Biomed Microdevices* **2008**, *10*, 367–374.
- (6) Curri, M. L.; Comparelli, R.; Striccoli, M.; Agostiano, A. *Phys. Chem. Chem. Phys.* **2010**, *12*, 11197.
- (7) Novikov, D. S.; Kozinsky, B.; Levitov, L. S. *Phys. Rev. B* **2005**, *72*, 235331.
- (8) Juna, S.; Jang, E.; par, J.; Kim, J. *Langmuir* **2006**, *22*, 2407–2410.
- (9) Lu, C.; Wu, N.; Wei, F.; Zhao, X.; Jiao, X.; Xu, J.; Luo, C.; Cao, W. *Adv. Funct. Mater.* **2003**, *13*, 548.
- (10) Park, J.-J.; Prabhakaran, P.; Jang, K. K.; Lee, Y.; Lee, J.; Lee, K.; Hur, J.; Kim, J.-M.; Cho, N.; Son, Y.; Yang, D.-Y.; Lee, K.-S. *Nano Lett.* **2010**, *10*, 2310–2317.
- (11) Tsuruoka, T.; Akamatsu, K.; Nawafune, H. *Langmuir* **2004**, *20*, 11169.
- (12) Son, J.; Bae, W. K.; Hang, H.; Nealy, P.; Char, K. *ACSNano* **2009**, *3*, 3927–3934.
- (13) Cui, Y.; Bjork, M. T.; Liddle, J. A.; Sonnichsen, C.; Boussert, B.; Alivisatos, A. *Nano Lett.* **2004**, *4*, 1093–1098.
- (14) Fanizza, E.; Malaquin, L.; Kraus, T.; Wolf, H.; Striccoli, M.; Micali, N.; Taurino, A.; Agostiano, A.; Curri, M. L. *Langmuir* **2010**, *26*, 14292–14300.
- (15) Hampton, M.; Templeton, J.; DeSimone, J. *Langmuir Letter* **2010**, *26*, 3012–3015.

- (16) Tekin, E.; Smith, P.; Hoepfener, S.; van den Berg, A. M. J.; Susa, A. S.; Rogach, A.; Feldman, J.; Schubert, U. *Adv. Funct. Mater.* **2007**, *17*, 23.
- (17) Tamborra, M.; Striccoli, M.; Curri, M. L.; Alducin, J. A.; Mecerreyes, D.; Pomposo, J. A.; Kehagias, N.; Reboud, V.; Torres, C. S.; Agostiano, A. *Small* **2007**, *3*, 822–828.
- (18) Mentzel, T. S.; Porter, V. J.; Geyer, S.; MacLean, K.; Bawendi, M. G.; Kastner, M. A. *Phys. Rev. B* **2008**, *77*, 075316.
- (19) Drndić, M.; Jarosz, M. V.; Morgan, N. Y.; Kastner, M. A.; Bawendi, M. G. *J. Appl. Phys.* **2002**, *892*, 7498.
- (20) Talapin, D.; Murray, C. *Science* **2005**, *310*, 86.
- (21) Yu, D.; Wang, C.; Guyot-Sionnest, P. *Science* **2003**, *300*, 1277.
- (22) Liljeroth, P.; Overgaag, K.; Urbieto, A.; Grandidier, B.; Hickey, S. G.; Vanmaekelbergh, D. *Phys. Rev. Lett.* **2006**, *97*, 096803.
- (23) Wills, A. W.; Kang, M. S.; Khare, A.; Gladfelter, W. L.; ; Norris, D. J. *ACS Nano* **2010**, *4*, 4523.
- (24) Porter, V. J.; Mentzel, T.; Charpentier, S.; Kastner, M. A.; Bawendi, M. G. *Phys. Rev. B* **2006**, *73*, 155303.
- (25) Jarosz, M. V.; Porter, V. J.; Fisher, B. R.; Kastner, M. A.; Bawendi, M. G. *Phys. Rev. B* **2004**, *70*, 195327–12.
- (26) Steckel, J.; Coe-Sullivan, S.; Bulovic, V.; Bawendi, M. *Advanced Materials* **2003**, *15*, 1862–1866.
- (27) Zhao, N.; Osedach, T. P.; Chang, L.-Y.; Geyer, S. M.; Wanger, D.; Binda, M. T.; Arango, A. C.; Bawendi, M. G.; Bulovic, V. *ACS Nano* **2010**, *4*, 3743.



- (28) Konstantatos, G.; Howard, I.; Fischer, A.; Hoogland, S.; Clifford, J.; Klem, E.; Levina, L.; Sargent, E. H. *Nature* **2006**, *442*, 180.
- (29) Strasfeld, D.; Dorn, A.; Wanger, D. D.; Bawendi, M. G. *Nano Lett.* **2012**, *12*, 569–575.
- (30) Mics, Z.; Němec, H.; Rychetský, I.; Kužel, P.; Formánek, P.; Malý, P.; Němec, P. *Phys. Rev. B* **2011**, *83*, 155326.

# Graphical TOC Entry

